Acta Metall. Sin. (Engl. Lett.)
DOI 10.1007/s40195-016-0458-2

Characteristics of the Structure and Properties of $ZnSnO_3$ Films by Varying the Magnetron Sputtering Parameters

Fa-Yu Wu[1] · Jian-Wei Li[1] · Yi Qi[2] · Wu-Tong Ding[3] · Yuan-Yuan Guo[1] · Yan-Wen Zhou[1]

Received: 22 February 2015 / Revised: 25 April 2015

Abstract Transparent conductive oxide $ZnSnO_3$ films were prepared by radio-frequency magnetron sputtering from powder targets and were characterized by X-ray photoelectron spectroscopy, X-ray diffraction, transmission electron microscopy, atomic force microscopy, surface profile, UV–Vis spectroscopy, and Hall effect. The structures of the films were either amorphous or nanocrystalline depending on sputtering parameters including deposition time, target power, chamber pressure, and the target–substrate separation. The average transmittance of the $ZnSnO_3$ films within the visible wavelength was approximately 80% and the resistivity of the $ZnSnO_3$ films was in the range of 10^{-3}–10^{-4} Ω cm. The structural, optical, and electrical properties of the $ZnSnO_3$ films could be adjusted and regulated by optimizing the sputtering process, allowing materials with specific properties to be designed.

KEY WORDS: $ZnSnO_3$ film; Powder target; Magnetron sputtering; Optical property; Electrical property

1 Introduction

Transparent conductive oxide (TCO) films are widely used in many fields including optoelectronic devices. Among the common TCO films, ITO (indium tin oxide) is recognized as having excellent optical and electrical properties; however, the indium consumed in ITO is a scarce resource and expensive. TCO films incorporating CdO are coming under environmental pressure due to the toxicity of cadmium. Therefore, TCO films based on ZnO or SnO_2, specially their multi-component films are becoming more attractive due to their low toxicity and lower cost [1–11].

Many techniques, such as magnetron sputtering, pulsed laser deposition, chemical vapor deposition, sol–gel, spray pyrolysis, cathodic electrodeposition, and inkjet-printing, are available to prepare multi-oxide TCO films. Among those deposition techniques, magnetron sputtering (MS) is one of the most practical means for preparing TCO films [4–8]. Studies on multi-component TCO films synthesized by closed-field unbalanced magnetron sputtering using powder targets in radio-frequency (RF) mode and pulsed direct current mode has been reported [12, 13]. Powder targets have the advantages of easily variable and controllable composition and low cost without the need of high temperature sintering process to prepare the target materials.

Several studies [7–10] showed that in the Zn–Sn–O system amorphous and nanocrystalline $ZnSnO_3$ and Zn_2SnO_4 films could be formed by PVD methods. Moreover, the crystalline and amorphous structures of these films could be regulated and controlled through variations in target power, substrate temperature and post annealing

Available online at http://link.springer.com/journal/40195

✉ Yan-Wen Zhou
photon_phonon@163.com

[1] Laser Advanced Manufacturing Technology Center, School of Materials and Metallurgy, University of Science and Technology Liaoning, Anshan 114051, China

[2] SINOTRUK (Hong Kong) Limited Jinan Casting and Forging Center, Zhangqiu 250200, China

[3] School of Material Science and Engineering, Shenyang University of Technology, Shenyang 110870, China

Published online: 02 July 2016

atmosphere and temperature. It is well known that the optical and electrical properties of multi-component TCO films depend on the chemical composition and the structure of the films, which in turn are determined by the preparation process. However, such relevance and dependence are not yet known well enough for Zn–Sn–O films prepared by MS from ZnO and SnO_2 mixed powders. In this study, mixture powders of ZnO and SnO_2 with the metallic atomic ratio of Zn:Sn = 1:1, were chosen as target materials in order to produce $ZnSnO_3$ films. The characteristics of the structure and properties of the $ZnSnO_3$ films were investigated by using an orthogonal experimental design approach in which the target power, chamber pressure, and target–substrate separation were chosen as the effect factors.

2 Experimental

$ZnSnO_3$ films were deposited in a rig which was specifically designed for powder target using. The 99.99% pure SnO_2 and ZnO powders with particle sizes in the range of 100 nm to 1 μm were mixed with the metallic atomic ratio of Zn:Sn = 1:1 and blended in a rotatable drum. The blended powders were then spread onto a copper plate to form a target with a uniform thickness and smooth compacted surface, as described in previous studies [12, 13]. The rig was evacuated to a base pressure lower than 3×10^{-3} Pa and then backfilled with argon gas to a pressure of 0.1, 0.3, or 0.5 Pa, depending on the array run settings (see Table 1). The sodium glass slides used as substrates, which were RF sputter cleaned in situ at 100 W for 15 min before deposition. The films were then deposited by RF sputtering at 200, 300, or 400 W for 4 h, and the target–substrate separations varied from 80 to 180 mm, again depending on the array run settings. The details of the L9 (3^3) experimental array is listed in Table 1, i.e., three factors at three levels ("low," "mid," and "high").

The structures of the films were subsequently characterized by transmission electron microscopy (TEM JEM 2100) at 200 kV, atomic force microscopy (AFM CSPM 3000) by contact mode, and X-ray diffraction (XRD X'Pert PRO) scanning with CuK_α radiation in θ–2θ mode. The through thickness metallic atomic ratio of the films was analyzed using X-ray photoelectron spectroscopy technique (XPS, Thermo Fisher Scientific K-Alpha). The film thicknesses were measured by an Afar-Step IQ Surface Profiler from step heights formed in the films by masking with tape. The electrical and optical properties were investigated according to the Van der Pauw method by using a SWIN Hall 8800 probe at room temperature and a UV-2802S spectrophotometer, respectively.

3 Results and Discussion

3.1 Film Composition

The composition of the $ZnSnO_3$ films was analyzed by XPS. The metallic atomic ratio through the thickness of the film was obtained while the film was sputtered in situ layer by layer. The signals for Zn2p^3 and Sn3d^5 remained stable through the thickness of the film, and the ratio of Zn:Sn was 1:1, as shown in Fig. 1, i.e., similar to that of the powder target. The proportion of oxygen in the films was about 44 at.%, which is much less than that in the target (60 at.%). According to the formula:

$$\lambda \propto 1/r^2, \tag{1}$$

where λ is mean free path and r is the radius of the atom, the mean free path of the small oxygen atom is much longer than those of the larger zinc and tin atoms under the

Table 1 Deposition parameters, electrical and optical properties of the $ZnSnO_3$ films (deposition time: 4 h)

Power (W)	P (Pa)	d_{ts} (mm)	d (nm)	N E + 19 (cm^{-3})	μ (cm^2 V^{-1} s^{-1})	ρ E-03 (Ω cm)	E_g (eV)
200	0.1	80	–	–	–	–	–
200	0.3	130	491	6.92	19.26	4.69	3.43
200	0.5	180	313	3.87	25.02	6.45	3.65
300	0.1	180	643	1.47	15.97	26.5	3.53
300	0.3	80	1717	21.1	15.95	1.85	3.23
300	0.5	130	1447	44.8	18.69	0.745	3.13
400	0.1	130	2661	52.2	16.75	0.75	3.20
400	0.3	180	1601	23.1	14.88	1.82	3.04
400	0.5	80	3724	203	16.72	0.184	2.62

P—pressure; d_{ts}—target–substrate separation; d—film thickness; N—carrier concentration; μ—carrier mobility; ρ—resistivity; E_g—optical band gap

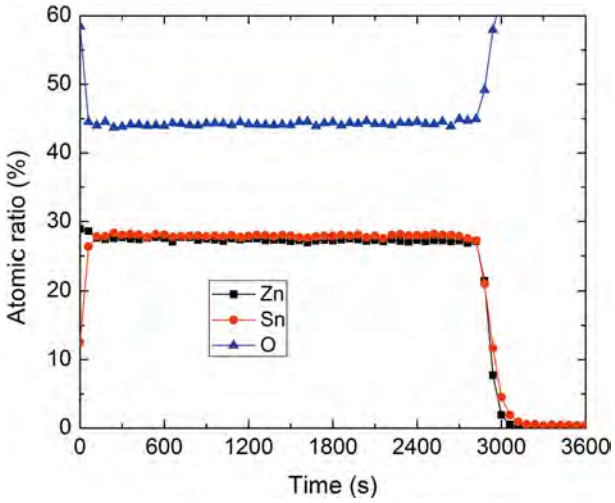

Fig. 1 Composition profile by XPS spectra through the thickness of the $ZnSnO_3$ film deposited at target power: 200 W, sputtering pressure: 0.5 Pa, target–substrate separation: 180 mm, Deposition time: 4 h

same pressure. Therefore, the oxygen atoms are more likely to be pumped out of the chamber making the oxide films oxygen deficient [14].

3.2 Film Structure

3.2.1 Crystallographic Structure

Figure 2 shows the XRD patterns of the films obtained with different process parameters. Figure 2a shows that there are two types of peak patterns in the XRD spectra of the $ZnSnO_3$ films prepared using the parameter array in Table 1. Some films show very diffuse diffraction peaks centered around $2\theta = 33.9°$ which are identified as $ZnSnO_3$ (110). This suggests that these films mainly consisted of amorphous $ZnSnO_3$. The other patterns include a broad peak at $2\theta = 36.6°$, identified as either the ZnO (101) or SnO_2 (200) peaks, which indicates evidence of ZnO and/or SnO_2 nanocrystallinity.

Studies of the stability and subgap states of crystalline and amorphous Zn–Sn–O by Körner [11] concluded that the formation energy of crystalline $ZnSnO_3$ was lower than that of amorphous $ZnSnO_3$. This means that crystalline $ZnSnO_3$ forms preferentially, and the probability of amorphous $ZnSnO_3$ formation would be greater if the energy delivered to the growing film was increased. It is well known that the substrate temperature would be increased and adatom mobility in the growing film would be increased under longer periods of ion bombardment. Therefore, the effect of deposition time on structure should not be neglected. Thus, films were prepared at the selected deposition parameters: 400 W–0.3 Pa–80 mm for 2 and 4 h to investigate the effect of the deposition time on the microstructure. Similar films were also deposited at 400 W–0.3 Pa–130 mm for 2 and 4 h to investigate whether mean free path had an additional influence on film structure. The XRD patterns in Fig. 2b suggest that nanocrystalline $ZnSnO_3$ formed preferentially for the short (2-h) deposition runs and the high (130-mm) separation runs, as indicated by the broad (110) diffraction peaks. In contrast, the long duration (4-h), low separation (80-mm) run resulted once again in a broad peak at $2\theta = 36.6°$, identified as either the ZnO (101) or SnO_2 (200) peaks. The film deposited for 4 h at a separation of 130 mm had a single highly diffuse peak indicative of an amorphous structure. These results imply that the formation of amorphous $ZnSnO_3$ and/or nanocrystalline ZnO and SnO_2 becomes more dominant during the higher energy deposition conditions of longer run time and shorter target–substrate separation. From these findings, it is reasonable to believe that the crystallographic microstructure of $ZnSnO_3$

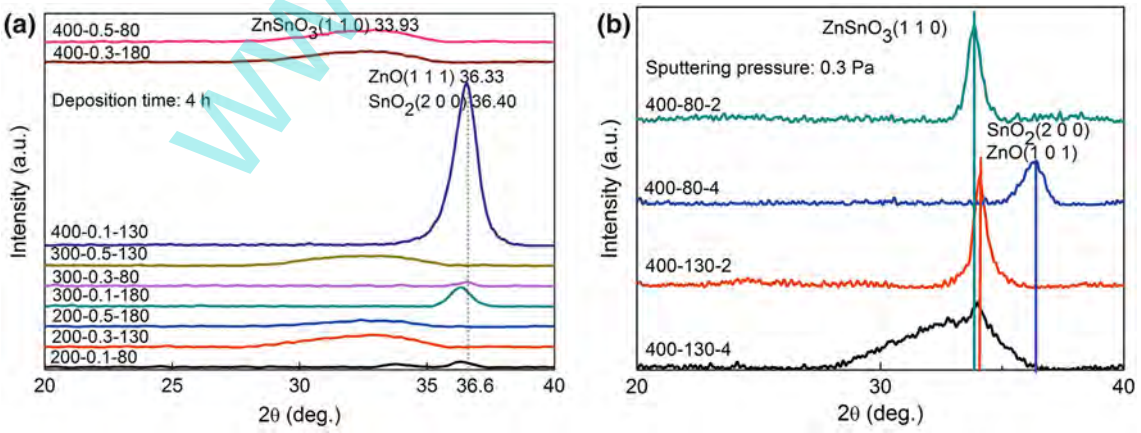

Fig. 2 XRD patterns of the $ZnSnO_3$ films **a** deposition conditions of Table 1; **b** target power: 400 W, sputtering pressure: 0.3 Pa, target–substrate separation: 80 and 130 mm, depositing time: 2 and 4 h, respectively

films could be adjusted by controlling the magnetron sputtering process from powder targets.

3.2.2 Microstructure and Morphology

Most of the TEM images show that the $ZnSnO_3$ films are amorphous or nanocrystalline, which is consistent with the above discussion from XRD. The TEM image of the film deposited at 400 W–0.3 Pa–130 mm for 2 h is especially shown in Fig. 3a. It can be seen that the sizes of the nanocrystalline domains of the film, revealed by the presence of lattice planes, are about 10–20 nm. The analysis of the selected area electron diffraction (SAED) pattern confirmed the formation of $ZnSnO_3$ grains with the appearance of (110) and (113) diffraction spots, illustrated in the inset to the figure. Moreover, the amorphous structure of the $ZnSnO_3$ film deposited for 4 h is shown in Fig. 3b to make a comparison.

Figure 4 shows the 3D AFM morphological images of selected $ZnSnO_3$ films. The grain size and roughness of the films were calculated using a CSPM image analyzer. The columnar grain sizes are over 150 nm, which consists of nanocrystalline domains or amorphous structure. The root-mean-square roughness of the films is of the order of 0.7–1.98 nm, which indicates that the surfaces of the $ZnSnO_3$ films are generally very smooth.

3.3 Film Thickness

The main effects of the array variables on film thickness, i.e., the deposition rate, are shown in Fig. 5a. It can be seen that the thickness is proportional to the sputtering power, as it would be expected. Also, the deposition rate of the $ZnSnO_3$ films decreases with increasing separation between the target and substrate, due to gas phase scattering as the coating atoms are transported through the discharge. Over the range testing, pressure had no significant effect on deposition rate.

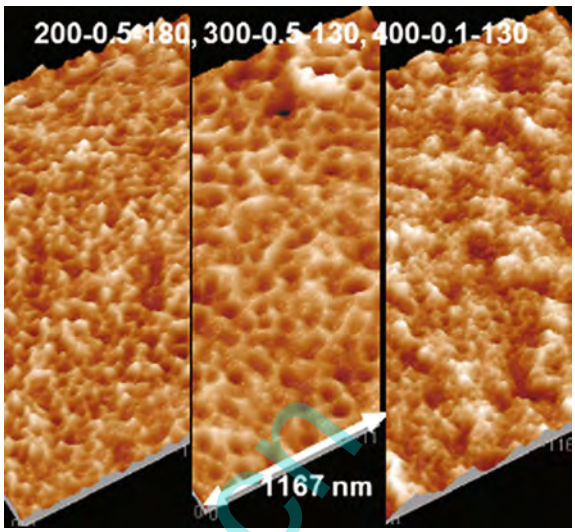

Fig. 4 Typical AFM morphology of the $ZnSnO_3$ films

3.4 Optical Properties

Figure 6 shows that the average transmittance within the visible wavelength range of the $ZnSnO_3$ films deposited at either 200 or 300 W is about 80%. That is lower than that of both ZnO and SnO_2 which show excellent transmittance values, normally over 90% [12, 15]. The transmittance of the films deposited at 400 W is much lower than those at 300 and 200 W. The possible reasons for such results are: (1) as discussed in Sect. 3.1, the stoichiometric ratio of the

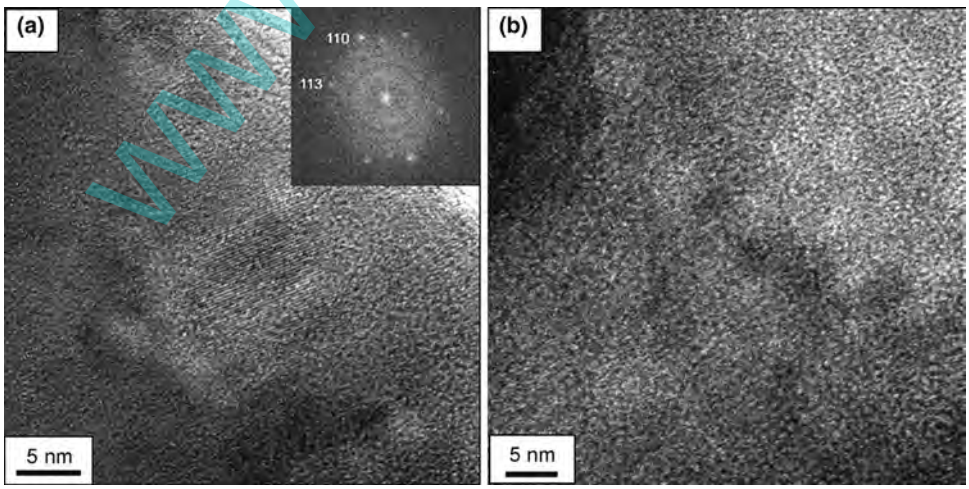

Fig. 3 **a** Nanocrystalline, **b** amorphous structure in TEM micrograph of the $ZnSnO_3$ deposited at 2 and 4 h, target power: 400 W, sputtering pressure: 0.3 Pa, target–substrate separation: 130 mm

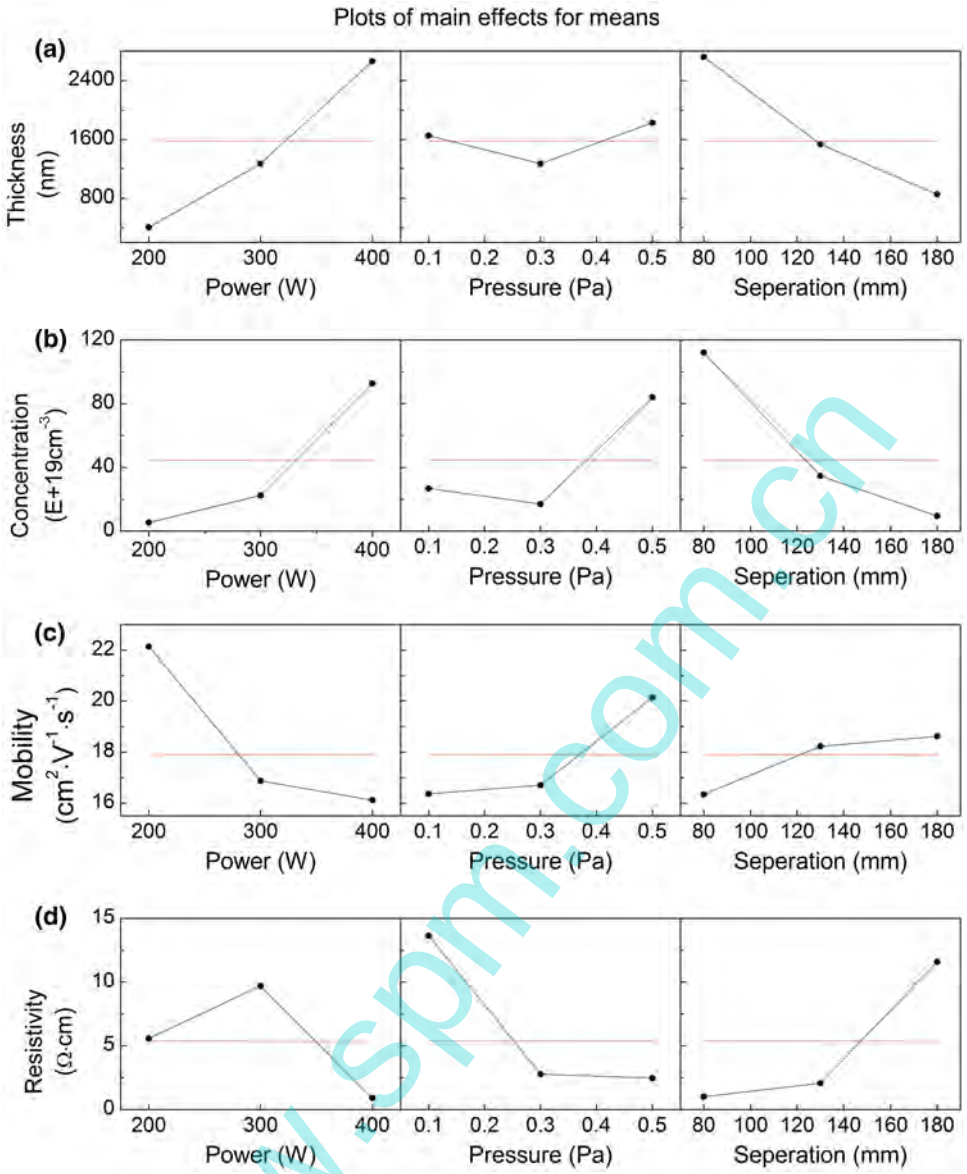

Fig. 5 Effects of the deposition parameter on the thickness and electrical properties by orthogonal analyses

$ZnSnO_3$ films is metal-rich due to the loss of oxygen atoms [14]. Consequently, the incident light is absorbed more due to the metallic tendency of the films and this effect is more prevalent at higher target powers. This is supported by the generally lower resistivity and greater thickness of the $ZnSnO_3$ films deposited at 400 W in Table 1. (2) It is usually hard for the transmittance of the incident light in the $ZnSnO_3$ films with the greater thickness.

The absorption coefficient (α) which represents the penetration depth of the incident photons is given by

$$\alpha = (1/d)\ln(1/T),$$

where T is transmittance and d is film thickness [16]. This equation assumes that the reflection is negligible.

The incident photon energy ($h\nu$) is given by

$$E = \hbar c/\lambda,$$

where $\hbar$ is Planck constant, equal to 4.136×10^{-15} eV s, c is the speed of light, 3×10^8 m/s, and λ is the wavelength of the incident light. The dependence of the absorption coefficient of $ZnSnO_3$ films was plotted as a function of the photon energy of the incident light. The optical band gap could be obtained by the linear extrapolation of the absorption coefficient curve and is listed as E_g in Table 1.

The optical band gaps of the $ZnSnO_3$ films became narrower with increasing target powers, as seen in Table 1. The lowest E_g value of 2.63 eV was obtained for the

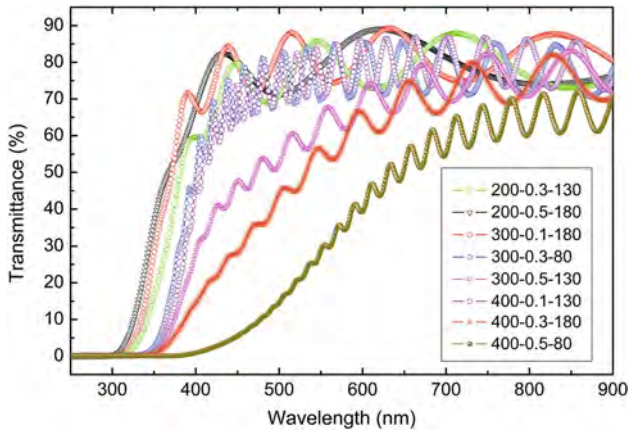

Fig. 6 Transmittance spectra of the $ZnSnO_3$ films

sample deposited at 400 W–0.5 Pa–80 mm. The high target power made the $ZnSnO_3$ films oxygen deficient. The subgap states in the upper part of the band gap could be caused by the oxygen vacancy related defects [11]. Furthermore, the high plasma density and energy provided to the growing films may lead to lattice deformations or atom arrangement disturbances. Therefore, both conductive and valence bands might be tailored and the optical band gap narrowed [3]. The optical band gaps narrowing implied that more electrons were able to be excited up to the conductive band and be set free. It should be reasonable to expect high carrier concentrations for $ZnSnO_3$ films deposited at high target power.

3.5 Electrical Properties

Based on the Hall effect, the electrical properties of the $ZnSnO_3$ films were measured and analyzed by the orthogonal statistics. The dependences of the electrical properties on the deposition parameters are outlined in Table 1 and illustrated in Fig. 5. All $ZnSnO_3$ films were n-type semiconductors, and electrons were the majority free charge carrier. The resistivity, charge carrier concentration and mobility of the films are in the range of 10^{-3}–10^{-4} Ω cm, 10^{19}–10^{20} cm^{-3} and 15–25 cm^2 V^{-1} s^{-1}, respectively, which are comparable to results published elsewhere [4, 8].

Figure 5b shows that the carrier concentration increased with the increase in target power and decrease of the target–substrate separation, which corresponded to films with lower optical band gaps. The narrow optical band gap meant it is easier for electrons to be excited into the conductive band, thus increasing the carrier concentration.

The high deposition rate conditions of high target power and low separation may also result in a distorted atomic arrangement in the films due to the increase of the plasma flux density and energy. According to the studies [7, 17] on binary oxide films that optical phonon scattering is the main action to affect the carrier mobility when the carrier concentration is within 10^{19}–10^{20} cm^{-3}, the transported electrons were scattered severely and the carrier mobility was reduced, as shown in Fig. 5c. In addition, the existence of nanocrystalline domain boundaries in the $ZnSnO_3$ films might further scatter the electrons and reduce their mobility.

As the chamber pressure increased, the plasma density became high and the plasma energy became low, respectively. As mentioned above, the high plasma density made $ZnSnO_3$ films bear more carriers while the low plasma energy caused the carriers in the films to be mobile. That is why both the carrier concentration and mobility increased with the increase of chamber pressure, as seen in Fig. 5b, c.

The statistical analysis of the resistivity of the $ZnSnO_3$ films as a function of the deposition parameters do not show a regular trend, as shown in Fig. 5d. The reason is that the resistivity is attributed to the combined action of both the carrier concentration and the carrier mobility [3, 4]. However, their dependences on the depositing parameters of $ZnSnO_3$ films are inconsistent sometimes. Anyway, the minimum resistivity was achieved from $ZnSnO_3$ film deposited by high target power, short target–substrate separation, and high chamber pressure. Moreover, $ZnSnO_3$ films for the different applications are expected to be prepared by selecting and optimizing deposition parameters.

4 Conclusions

$ZnSnO_3$ films were prepared by varying magnetron sputtering parameters from ZnO and SnO_2 mixed powder targets. $ZnSnO_3$ nano-crystalline phases in the columnar grains formed preferentially for the films deposited in short deposition time of 2 h. Extending the deposition time to 4 h, the growth of the films transformed from nanocrystalline $ZnSnO_3$ to either amorphous $ZnSnO_3$ or nanocrystalline of ZnO and SnO_2. With increasing target power and decreasing target–substrate separation, the deposition rate of the film thickness increased and the optical band gap of the films narrowed, then carrier concentration increased but carrier mobility of the films decreased. Comparatively, the chamber pressure was the weaker effect factor in this study. On the whole, the average transmittance within the visible wavelength of $ZnSnO_3$ films was about 80%. Meanwhile, the optical band gap and the resistivity of $ZnSnO_3$ films were at the range of 2.6–3.4 eV and 10^{-3}–10^{-4} Ω cm, respectively.

Acknowledgments This work was financially supported by the National Natural Science Foundation of China (Nos. 51372109 and 51502126), and the Foundation of Educational Department of Liaoning (No. L2015260), and the Open Subject of Key Laboratory Liaoning Province (No. USTLKFSY201501).

References

[1] B. Szyszka, W. Dewald, S.K. Gurram, A. Pflug, C. Schulz, M. Siemers, V. Sittinger, S. Ulrich, Curr. Appl. Phys. **12**, S2 (2012)
[2] K.P. Ong, X.F. Fan, A. Subedi, M.B. Sullivan, D.J. Singh, APL Mater. **3**, 062505-1 (2015)
[3] L.J. Huang, N.F. Ren, B.J. Li, M. Zhou, Acta Metall. Sin. (Engl. Lett.) **28**, 281 (2015)
[4] Damisih, H.C. Ma, J.J. Kim, H.Y. Lee, Thin Solid Films **520**, 3741 (2012)
[5] N. Yasrebi, B. Bagheri, P. Yazdanfar, B. Rashidian, P. Sasanpour, Acta Metall. Sin. (Engl. Lett.) **27**, 324 (2014)
[6] J.H. Ko, I.H. Kim, D. Kim, K.S. Lee, T.S. Lee, B. Cheong, W.M. Kim, Appl. Surf. Sci. **253**, 7398 (2007)
[7] R. Mamazza Jr., D.L. Morel, C.S. Ferekides, Thin Solid Films **484**, 26 (2005)
[8] I.J. Lee, N.E. Sung, K.H. Chae, R. Conley, Thin Solid Films **548**, 385 (2013)
[9] R. Acharya, Y.Q. Zhang, X.A. Cao, Thin Solid Films **520**, 6130 (2012)
[10] J.H. Ko, I.H. Kim, D. Kim, K.S. Lee, T.S. Lee, J.H. Jeong, B. Cheong, Y.J. Baik, W.M. Kim, Thin Solid Films **494**, 42 (2006)
[11] W. Körner, C. Elsässer, Thin Solid Films **555**, 81 (2014)
[12] P.J. Kelly, Y. Zhou, J. Vac. Sci. Technol., A **24**, 1782 (2006)
[13] Y. Zhou, P. Kelly, Q.B. Sun, Thin Solid Films **516**, 4030 (2008)
[14] A. Chambers, R.K. Fitch, B.S. Halliday, *Basic Vacuum Technology*, 2nd edn. (IOP Publishing Ltd., UK, 1998), p. 10
[15] Y. Zhou, F. Wu, C. Zheng, Chin. Phys. Lett. **28**, 107307 (2011)
[16] M.M. El-Nahass, A.A. Atta, M.M.A. El-Raheem, A.M. Hassanien, J. Alloys Compd. **585**, 1 (2014)
[17] G.J. Exarhos, X.D. Zhou, Thin Solid Films **515**, 7025 (2007)